ACS OMEGA

Article

Cite This: ACS Omega 2019, 4, 3146−3158

http://pubs.acs.org/journal/acsodf

Design and Exploration of Catalytic Activity of Two-Dimensional Surface-Engineered Graphene Oxide Nanosheets in the Transannulation of N-Heterocyclic Aldehydes or Ketones with Alkylamines

Rakesh K. Sharma,* Aditi Sharma, Shivani Sharma, Sriparna Dutta, Sneha Yadav, and Bhavya Arora

Green Chemistry Network Centre, Department of Chemistry, University of Delhi, New Delhi 110007, India

Supporting Information

ABSTRACT: In this work, pharmaceutically and biologically important compounds containing imidazo[1,5-*a*]pyridine nuclei have been synthesized via transannulation of N-heteroaryl aldehydes or ketones with alkylamines using a graphene oxide-supported copper catalyst. The nanocatalyst was fabricated by the covalent immobilization of 4-aminoantipyrine onto an amine-functionalized graphene oxide nanosupport followed by its metallation with copper acetate. Structural analysis by transmission electron microscopy, scanning electron microscopy, X-ray photoelectron spectroscopy (XPS), and X-ray diffraction demonstrates that the two-dimensional sheet-like structure of graphene oxide is maintained even after the chemical modifications, whereas XPS revealed crucial information related to elemental composition and surface electronic states of the metal present in the catalyst. Apart from this, Fourier transform infrared spectroscopy helped in identifying the degree of oxidation and the presence of oxygenated groups in graphene oxide nanocomposites. As a heterogeneous catalyst, this graphene oxide-supported copper complex showed moderate to good catalytic activity in the C(sp^3)−H bond activation/amination of a variety of substrates. This superior catalytic performance originated from the unique 2-dimensional structure of graphene oxide-based material which provided space between graphitic overlayers due to appropriate positioning of metal on their basal planes, decreasing the diffusion resistances of reactant surfaces, thus making it function as a nanoreactor. More importantly, this nanomaterial could be recovered easily and reused repeatedly by simple washing without chemical treatment with no appreciable loss in its catalytic activity, showing good potential for increasing the overall turnover number of this synthetically useful catalyst.

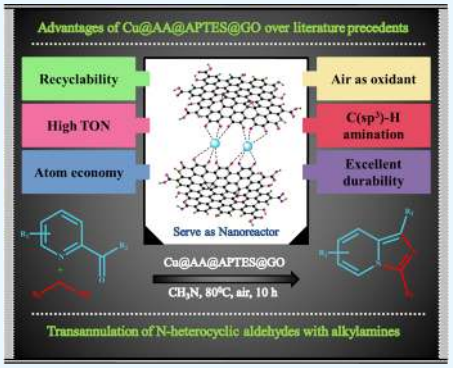

INTRODUCTION

Transition-metal-catalyzed C−H amination represents an attractive strategy for the synthesis of nitrogen-containing heterocyclic compounds as it provides undeniable benefits of high atom economy and reduced waste generation, which cause such reactions to fall under the banner of green chemistry.[1−3] Although a noteworthy advancement in the C(sp^2)−H bond activation strategy enabling C(sp^2)−N bond formation has been witnessed in recent years,[4−7] yet the catalytic functionalization of the relatively inert C(sp^3)−H bonds which can provide a unique access to site-selective C−N bonds remains a major challenge in synthetic organic chemistry.[8−13] To accomplish C(sp^3)−H bond activation, various amine sources have been scrutinized which include arylamines and aliphatic amines, amides, azides, haloamines, and so forth in the presence of suitable transition-metal catalysts. Recently, N-heteroarenes have proven their efficacy as an excellent amino source for the metal-catalyzed C(sp^3)−H amination.[14−17]

Imidazo[1,5-*a*]pyridine scaffolds are a class of nitrogen-bridgehead-fused heterocycles, present in several pharmacologically important molecules that unveil a broad spectrum of biological activities such as antimicrobial, antineoplastic, antianxiety, anti-inflammatory, and so forth.[18−21] Apart from comprising intrinsic exceptional biological and pharmacological properties, these compounds also serve as expedient predecessors for a variety of functional group transformations. To date, a paucity of approaches have been reported to construct imidazo[1,5-*a*]pyridines fundamentally relying on the Vilsmeier-type protocol and Wallach imidazole synthesis.[22−24] Nevertheless, none of the methodologies enlisted in the literature are environmentally benign because they inevitably involve the use of either excess amount of additives, active starting materials, or multistep processes.[25−30] Therefore, the development of new flexible, atom-economic, and proficient protocols for these imidazo[1,5-*a*]pyridines is of upsurge interest. In this direction, copper-catalyzed direct transannulation of N-heteroaryl aldehydes or ketones with

Received: December 1, 2018
Accepted: January 23, 2019
Published: February 12, 2019

DOI: 10.1021/acsomega.8b02902
ACS Omega 2019, 4, 3146−3158

Scheme 1. Schematic Illustration for the Synthesis of Cu@AA@APTES@GO Nanocatalyst

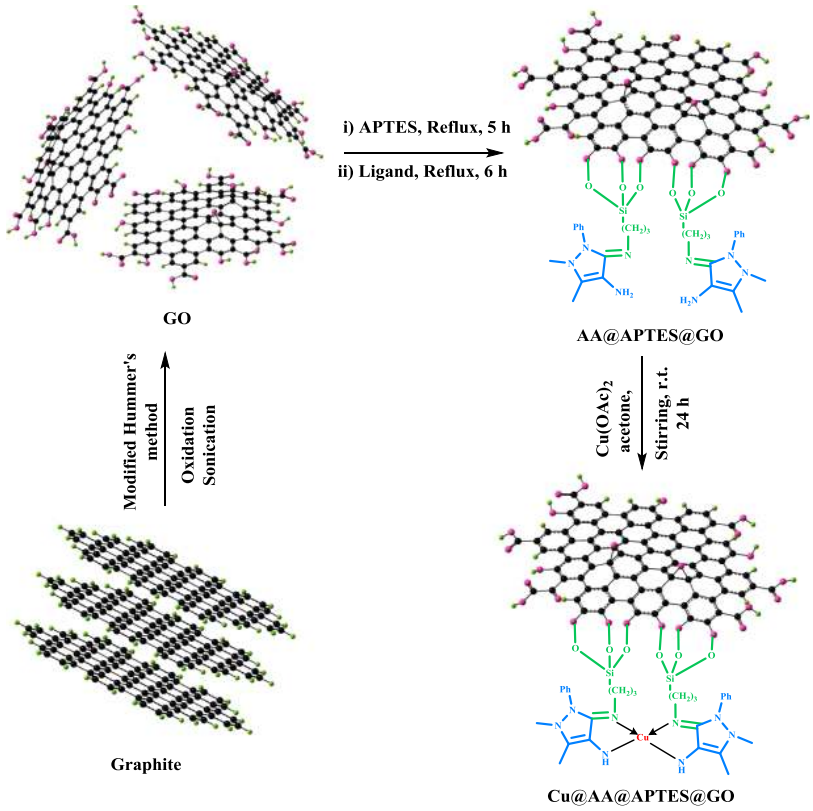

alkylamines that involves a oxidative C(sp^3)−H activation strategy has attracted the synthetic pursuit of research studies as it represents one of the most powerful gateways to obtain a diverse range of the substituted imidazo[1,5-*a*]pyridines simply through one-pot condensation−amination−oxidative dehydrogenation process.[31−35] Though the homogeneous copper catalysts offer high conversion percentage, selectivity, and yields under relatively mild operating conditions, but their industrial applicability is hampered by the inherent problem of catalyst separation from the reaction mixture and its recyclability. Moreover, the presence of copper residues in the product stream renders its commercial utility rather desolate in the pharmaceutical industries. In view of these severe limitations, there is an urgent need to develop novel retrievable catalytic systems that can surmount the challenges of homogeneous catalysis and also preserve the best attributes of both homogeneous and heterogeneous catalysts for the generation of a library of imidazo[1,5-*a*]pyridine nuclei.

The introduction of novel nanotechnologies has empowered the generation of solid-supported heterogeneous nanoscale catalysts, which are effective tools for controlling chemical reactivity as well as facile recovery.[36−43] Amongst a multitude of solid nanostructures enlisted in the literature, two-dimensional (2D) graphene oxide in particular offers excellent prospects to provide a platform for such third-generation catalytic systems owing to their exceptional structural properties such as nanometer size, excellent chemical and thermal stability, good accessibility, porosity, and large surface area-to-volume ratio. In addition, these nanosheets provide the opportunity to tune the structure of the catalyst via chemical modifications because of the presence of numerous hydroxyl, epoxy, carboxyl, and carbonyl groups on its surface which allow the immobilization of a diverse array of reagents and also intensify their use in different chemical transformations.[44−48]

Our recent fast-growing research focused on the development of sustainable organic−inorganic hybrid nanomaterials motivated us to come up with new graphene oxide-based retrievable 2D nanocatalytic system that substantiated their efficiency in C(sp^3)−H activation for direct transannulation of N-heteroaryl aldehydes or ketones with alkylamines using molecular oxygen as an oxidant.[49−54] This novel nanostructured catalyst not only demonstrates benefits such as the ease of product separation but can also be used for multiple runs without any appreciable loss in its catalytic activity. The reason behind the good catalytic efficacy can be attributed to chemically modified graphene oxide that forms crumpled nanosheets/nanostacks which provide engineered internal cavities creating unique incarcerate nanoscale environments for chemical reactions. Moreover, utilization of molecular oxygen as an environmentally benign oxidant to achieve this oxidative transformation functions as a prevailing tool to enhance the sustainability of chemical process as there is no formation of side product. To the best of our knowledge, this report is the first example of atom economical and environmentally benign C−H amination wherein a graphene oxide-based copper catalyst has been effectively exploited for the synthesis of pharmaceutically and biologically significant compounds.

EXPERIMENTAL SECTION

Materials and Reagents. Graphite flakes (Sigma-Aldrich), 3-aminopropyltriethoxysilane (APTES, Alfa Aesar), and 4-aminoantipyrine (AA) (Spectrochem Pvt. Ltd, India) were commercially procured. All other reagents and solvents

DOI: 10.1021/acsomega.8b02902
ACS Omega 2019, 4, 3146−3158

employed for the synthesis were of analytical grade and used as received.

Characterization Techniques. Transmission electron microscopy (TEM) analysis was carried using a Tecnai G2 T30 microscope in order to determine the morphology of nanosheets. Field emission scanning electron microscopy (FESEM) images were obtained in order to derive information about the morphological characteristics of nanosheets using a Tescan Mira 3 FESEM instrument. Energy-dispersive X-ray spectroscopic (EDS) analysis equipped with the FESEM (Zeiss FESEM) was achieved for the elemental mapping of the nanocomposites. Fourier transform infrared (FT-IR) spectra were acquired through a PerkinElmer Spectrum 2000 using the KBr pellet method that was operative in the range of 4000−500 cm^{-1} under atmospheric conditions with a resolution of 1 cm^{-1}. Powder X-ray diffraction (XRD) was carried out using a Rigaku Ultima (IV) diffractometer with Cu Kα radiation at a scanning rate of 2° min^{-1} in the 2θ range of 8−80° (40 kV, 40 mA). Energy-dispersive X-ray fluorescence (ED-XRF) spectroscopy was performed using a Fischerscope X-ray XAN-FAD BC. The copper content in the nanocatalyst was estimated by using a flame atomic absorption spectrometer (model no. N3180021 PinAAcle 500) using an acetylene flame. All of the derived products were examined through the gas chromatography−mass spectrometry (GC−MS) hyphenated technique that was conducted utilizing the Agilent gas chromatograph (6850 GC) with a HP-5MS 5% phenyl methyl siloxane capillary column (30.0 m × 250 μm × 0.25 μm) and a quadrupole mass filter equipped 5975 mass selective detector using helium as the carrier gas.

Preparation of Organoamine-Functionalized Graphene Oxide Nanocomposites (APTES@GO). GO was prepared by the oxidation of graphite powder via the modified Hummers' method.[55] For obtaining amine-functionalized graphene oxide (APTES@GO) nanocomposites, APTES (2 mmol) was added dropwise to a well-dispersed solution of GO (1.0 g) in ethanol (200 mL) and stirred under reflux conditions for 5 h.[56] The resulting mixture was separated via centrifugation, washed several times with ethanol to remove residual APTES, and dried under vacuum overnight.

Synthesis of Graphene Oxide Nanosheet-Based Copper Catalyst (Cu@AA@APTES@GO). The final synthesis of the Cu@AA@APTES@GO nanocatalyst was carried out using a two-step procedure. First, organoamine-functionalized graphene oxide (0.5 g) was dispersed in ethanol (30 mL) using an ultrasonic bath. Thereafter, AA was added to suspension and stirred under reflux conditions for 6 h in order to obtain AA@APTES@GO.[57] In the next step, AA@APTES@GO was added to a solution containing copper acetate (1.5 mmol) in acetone (100 mL) and stirred at room temperature for 24 h. The resulting nanocomposites were removed through centrifugation, washed thoroughly with ethanol, and dried under vacuum to obtain the Cu@AA@APTES@GO nanocatalyst (Scheme 1).[58,59]

General Procedure for the Reaction. A mixture of 2-acetylpyridine (0.10 mmol) and benzyl amine (0.10 mmol) was refluxed at 80 °C in the presence of the Cu@AA@APTES@GO nanocatalyst (15 mg) using acetonitrile (2 mL) as a solvent and then stirred for the desired reaction time. The progress of the reaction was monitored by thin-layer chromatography (ethyl acetate−hexane). After completion of reaction, the mixture was allowed to cool to room temperature and the nanocatalyst was recovered via centrifugation. Then, the reaction mixture was quenched with water and extracted with ethyl acetate. The combined organic layers were separated and dried over Na_2SO_4, and the solvent was removed under vacuum. The products obtained were thereafter analyzed and confirmed by GC−MS.

RESULTS AND DISCUSSION

Motivation and Strategy. Considering the scarcity of sustainable methods integrating efficiency, selectivity, and reusability in a single platform, through the present work, we report graphene oxide-supported copper catalyst for the synthesis of imidazo[1,5-*a*]pyridines. The utilization of the 2D heterostructure of the catalytic material that provides intriguing confined space between graphitic overlayers and metal surfaces enables it to function as a nanoreactor, thereby playing an indispensable role in expediting this reaction and affording the target products with good to excellent yield. Also, the extremely high thermal conductivity of graphene oxide allows conduction and diffusion of the heat produced during catalytic reactions that makes it a good candidate for the support matrix.

FT-IR Spectroscopy. The FT-IR spectra of GO, APTES@GO, AA@APTES@GO, and Cu@AA@APTES@GO are demonstrated in Figure 1. FT-IR spectroscopy identifies the

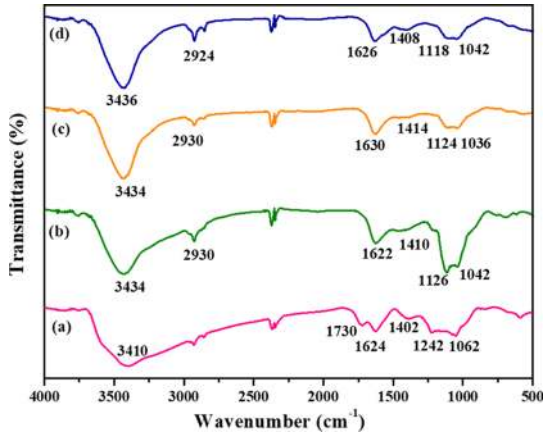

Figure 1. FT-IR spectra of (a) GO, (b) APTES@GO, (c) AA@APTES@GO, and (d) Cu@AA@APTES@GO.

degree of oxidation and presence of the oxygenated species in GO. In the spectrum of GO, the characteristic peaks at 3410, 1730, 1624, 1402, and 1062 cm^{-1} are due to the OH, C═O in −COOH, aromatic C═C, carboxy C−O, and epoxy C−O stretches, respectively, situated at the edges of GO nanosheets.[60] Thereafter, the covalent functionalization of the nanosupport with APTES is confirmed through the presence of additional absorption band at 2930 cm^{-1} which is assigned to stretching vibrations of C−H bonds, whereas the bands at 1622 and 3434 cm^{-1} that can be attributed to N−H stretching and bending vibrations. The sequential introduction of ligand (AA) to the silane terminal by condensation with apical amine groups is verified by the appearance of a strong band at 1630 cm^{-1} which is associated with the stretching vibrations of C═N. Consistent with this interpretation, a noticeable shift (1626 cm^{-1}) in the imine vibrations of the Schiff base which can be accredited to electron delocalization of C═N and coordination interaction with the copper metal.[61] These results confirm

DOI: 10.1021/acsomega.8b02902
ACS Omega 2019, 4, 3146−3158

the successful anchoring of copper complex onto the GO surface as Cu@AA@APTES@GO.

XRD Analysis. XRD analysis was done in order to investigate the phase structure and crystallinity of the nanocomposites. Figure 2 depicts that graphite powder exhibits

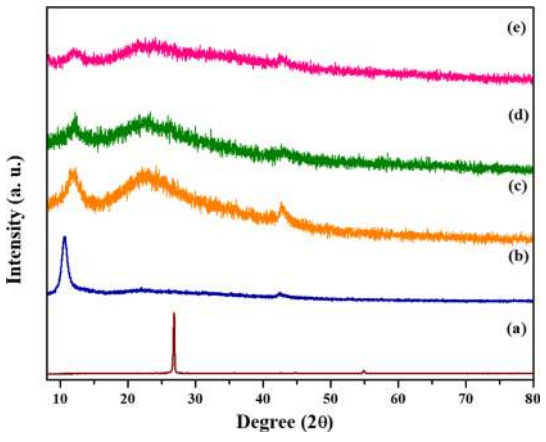

Figure 2. Powder XRD of (a) graphite, (b) GO, (c) APTES@GO, (d) AA@APTES@GO, and (e) Cu@AA@APTES@GO.

a high degree of crystallinity with an intense and sharp diffraction peak at $2\theta = 26.8°$ which corresponds to the crystal plane (002) with an interplanar distance of 0.33 nm.[62] In contrast, unmodified GO shows a lower degree of crystallinity with a small broad diffraction peak at $2\theta = 10.7°$ having *d*-spacing 0.825 nm corresponding to the (001) crystal plane.[63] Clearly, the increase in the interlayer distance of graphene oxide indicates the hydration and exfoliation of GO in an aqueous medium which revealed the formation of various oxygen containing functionalities such as hydroxyl, epoxy, carbonyl, carboxyl groups, and so forth. After the immobilization of aminopropyl moiety on GO nanosheets, the diffraction peak at around 10.7° does not disappear, suggesting that the structure of GO is not destroyed; however, a decrease in the intensity of this peak can be observed along with the appearance of a new peak around 22°.[64] Moreover, ligand-grafted amine-functionalized graphene oxide and final nanocatalyst showed further decrease in the intensity of both of these diffraction peaks. The decrease in the intensity of the diffraction peak of GO with successive surface modifications could be attributed to the intercalation of functional groups, suggesting the decrease in ordered arrangement of GO nanosheets.[65−67]

Morphology Analysis. FESEM and TEM are powerful magnification tools which provide detailed information about the evolution of morphology, composition, and texture of nanocomposites. The nanomaterials, both before and after grafting, were also characterized by FESEM and TEM. As displayed in Figure 3, it can be visualized that GO inherits twisted 2D planar morphology. Further, as we move from GO to APTES@GO to Cu@AA@APTES@GO, the extent of crumpling and protrusions increases which provide evidences for enormous surface area of nanomaterials. Therefore, these lamellar folded flakes (well-stacked layered structure) with wrinkles induce not only high degree of active catalytic sites but also serve as a versatile platform for efficient chemical transformations. Besides, a thorough analysis of TEM micrograph of GO confirms the corrugated sheet-like nature of material with a lateral dimension up to several micrometers. Further, it is observed that even after the surface modification with organic functionalization moieties, the corrugated sheet-like structure of GO nanocomposites is maintained. Apart from this, the selected-area electron diffraction pattern of GO shown in the inset of Figure 3f shows sharp diffraction spots indicating amorphous nature of GO flakes.[68−70] Additionally, SEM and TEM images of the recovered nanocatalyst do not show any change in their crumpled morphology, suggesting that the catalyst is robust enough to withstand the applied reaction conditions (Figures S1 and S2).

X-ray Photoelectron Spectroscopy. X-ray photoelectron spectra of Cu@AA@APTES@GO are presented in Figure 4. The surface electronic states and the interactions of chemically modified GO were assessed by X-ray photoelectron spectroscopy (XPS). The appearance of a band around 286.2 eV

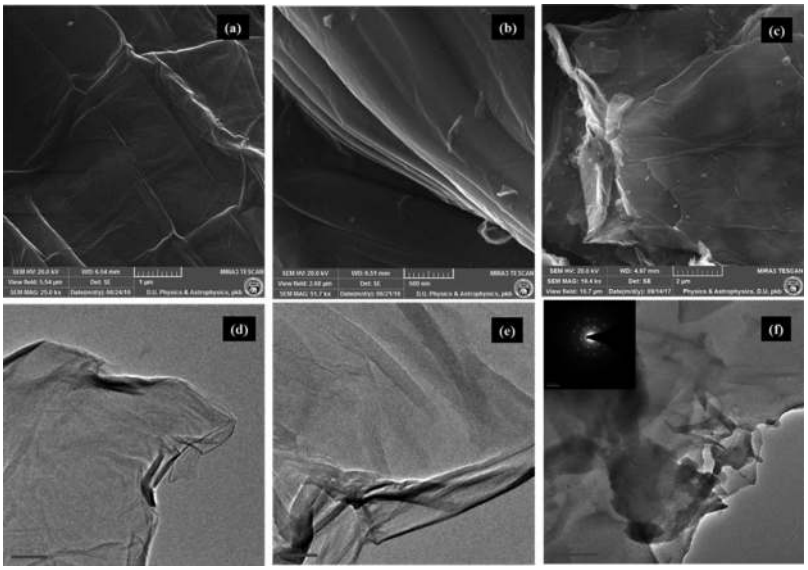

Figure 3. FESEM micrographs of (a) GO, (b) APTES@GO, and (c) Cu@AA@APTES@GO and TEM micrographs of (d) GO, (e) APTES@GO, and (f) Cu@AA@APTES@GO.

DOI: 10.1021/acsomega.8b02902
ACS Omega 2019, 4, 3146−3158

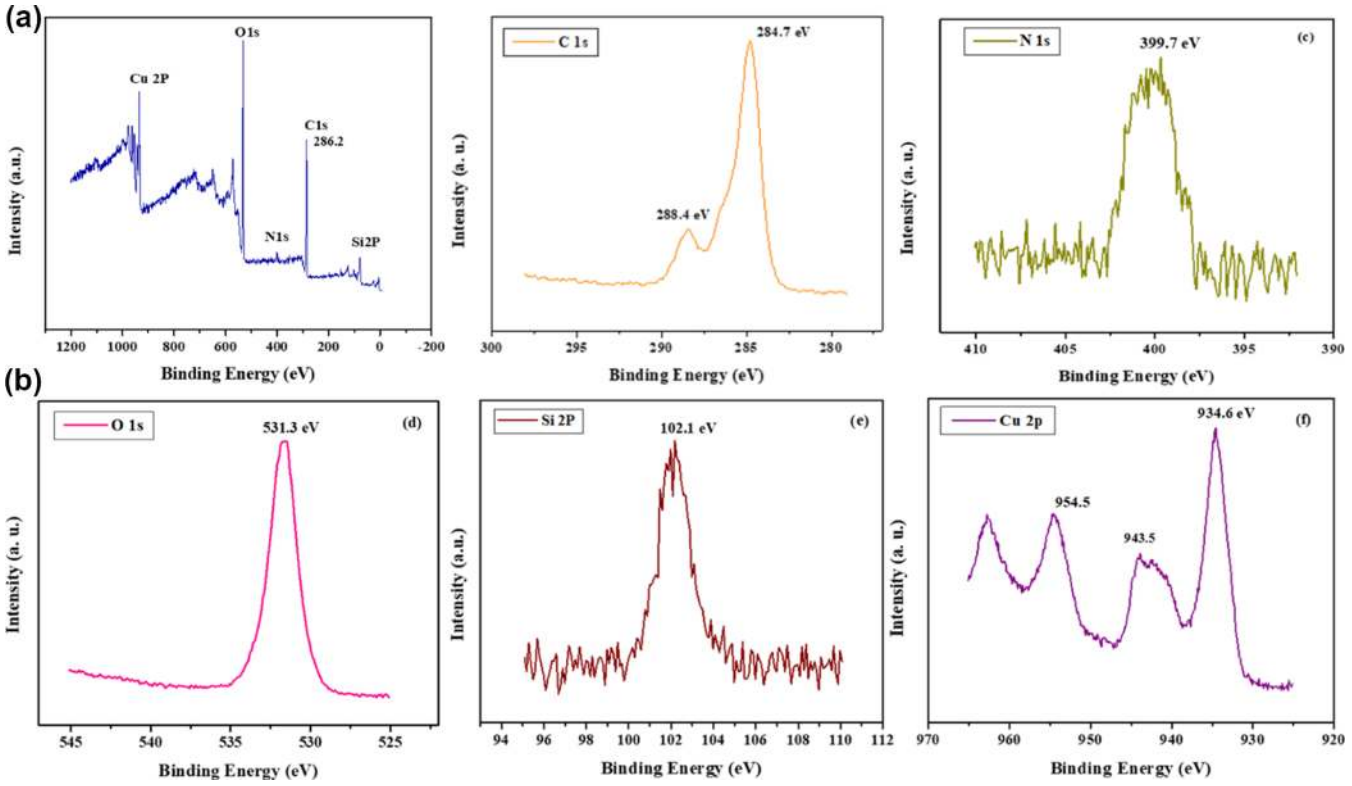

Figure 4. Full-range XPS spectra of (a) Cu@AA@APTES@GO and core-level spectra of (b) C 1s, (c) N 1s, (d) O 1s, (e) Si 2p, and (f) Cu 2p spectra of the nanocatalyst.

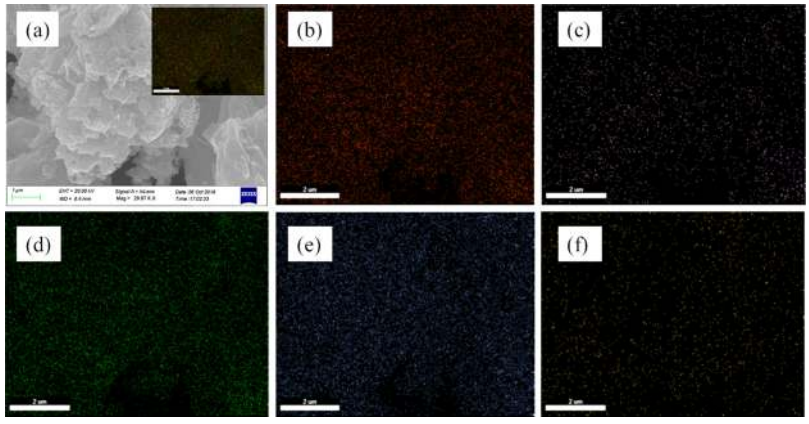

Figure 5. (a) FESEM image Cu@AA@APTES@GO of the catalyst and corresponding elemental mapping images of (b) carbon, (c) nitrogen, (d) oxygen, (e) silicon, and (f) copper.

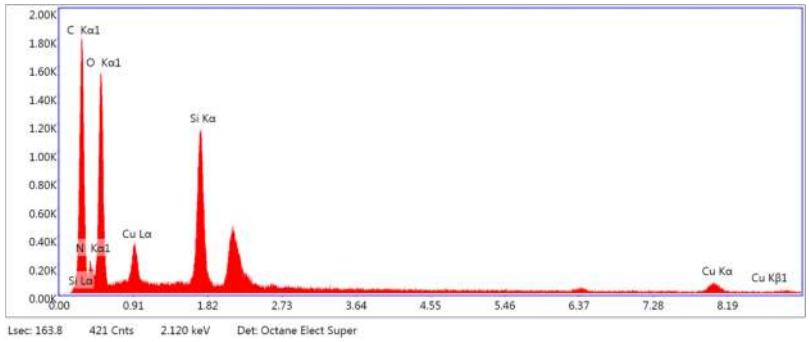

Figure 6. EDS spectra of the Cu@AA@APTES@GO catalyst.

DOI: 10.1021/acsomega.8b02902
ACS Omega 2019, 4, 3146−3158

designates C−O−C and C−OH bonds which indicate a considerable degree of oxidation and the presence of different oxygen-containing groups. In addition, the C 1s spectrum of the catalyst reveals two more bands at 284.7 that correspond to C−H and C−C bonds and 288.4 eV which arises from O−C═O bonds. Besides, new bands at 399.4, 400.8, and 401.33 emerging in the N 1s spectrum are attributed to C−N═C, C−N−H, and ═N−, respectively (Figure S3). Moreover, the presence of a band at 102.1 eV accredited to Si−O arises in the Si 2p spectrum. This designates the silylation reaction between silanol group of APTES and GO surface hydroxyl groups. Further, the Cu 2p XPS spectrum of the nanocatalyst shows two typical bands at 934.6 and 954.5 eV, which correspond to the binding energies of copper(II). In addition, a Cu $2p_{3/2}$ satellite peak appearing at 943.5 eV explained the coordination interaction between the ligand and the copper center.[71,72]

Elemental and Compositional Analysis. The composition of nanostructured GO-supported catalyst was also confirmed by EDS (Figures 5, 6, and S4) and ED-XRF spectroscopy (Figure S5). EDS elemental mapping images of the graphene oxide-supported copper catalyst clearly show the presence of all of the elements, that is, Cu, C, N, Si, and O on the surface of the GO nanosheets which provides the evidence for the successful organoamine functionalization, ligand grafting, and metallation. Further, a well-resolved peak of copper in the ED-XRF spectrum of Cu@AA@APTES@GO also confirms the successful metallation of AA@APTES@GO.[73] Subsequently, the quantitative estimation of the copper content in the synthesized nanocatalyst was done after digestion using atomic absorption spectroscopy, and the corresponding copper loading was estimated to be 0.126 mmol g^{-1}.

Raman Spectroscopy. Raman spectroscopy is a powerful technique to study the structural and chemical changes in the obtained nanomaterials. The Raman spectra of GO, APTES@GO, AA@APTES@GO, and Cu@AA@APTES@GO are shown in Figure 7. The presence of two characteristic peaks centered at 1597 and 1347 cm^{-1} is attributed to G and D bands of GO which are associated with the vibrations of sp^2 bonded carbon networks.[74,75] Further, chemical modifications of GO are confirmed by comparing the intensity ratio of D and G bands (I_D/I_G). The increase in the I_D/I_G ratio from 0.98 to 1.01, 1.04, and 1.05 confirms the stepwise covalent anchoring of aminosilane chain, ligand grafting, and metallation onto the surface of GO.[76]

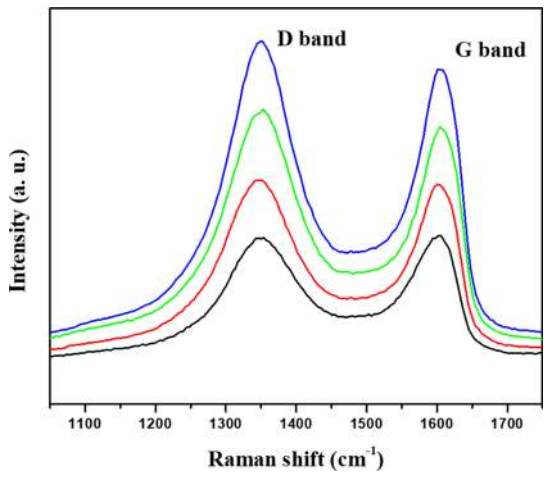

Figure 7. Raman spectra of GO (black), APTES@GO (red), AA@APTES@GO (green), and Cu@AA@APTES@GO (blue).

Optimizations. Initial optimization studies for transannulation of N-heteroaryl aldehydes or ketones were carried out using 2-acetylpyridine and benzyl amine as standard substrates. The presence of the catalyst was found to be necessary because no appreciable amount of the product was detected in its absence. Thereafter, we employed different catalysts for affording the desired product (Table S1). The highest conversion percentage was obtained in the case of the Cu@AA@APTES@GO nanocatalyst, suggesting the efficiency of the graphene oxide-based copper nanocomposites for C(sp^3)−H amination (Figure S8).

Amount of the Catalyst. The key parameter to evaluate the catalytic performance is the effect of the amount of the catalyst. In order to evaluate its effect on model reaction, we carried out six experiments in which we simply increased the amount of the catalyst from 5 to 30 mg. It was observed that the 100% conversion was obtained when the amount of the Cu@AA@APTES@GO nanocatalyst was increased from 5 to 15 mg (Figure 8). Further, it was observed that the conversion

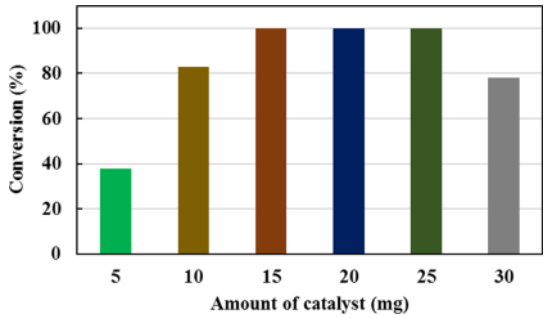

Figure 8. Effect of amount of the catalyst on the transannulation of N-heteroaryl aldehydes or ketones [reaction conditions: 2-acetylpyridine (0.10 mmol), benzyl amine (0.10 mmol), acetonitrile (2 mL), catalyst (x mg), 10 h, 80 °C].

percentage remained same on increasing the amount of the catalyst up to 25 mg. However, on increasing the amount of the catalyst to 30 mg, conversion percentage decreased because of the low dispersity of the excess catalyst in the reaction media which is caused due to steric hindrance of the mass transfer between the active site and reagent. Therefore, the best result was obtained when the reaction was performed using 15 mg of the nanocatalyst.

Effect of Time. The catalytic efficacy of Cu@AA@APTES@GO in the transannulation of N-heterocyclic aldehydes was studied at different time intervals. The conversion percentage has been represented as a function of time in Figure 9. A close comparison of results revealed that the conversion percentage increased from 25 to 100% as time was increased from 2 to 10 h. Further, when the reaction was continued for 12 h, no significant change was observed. Therefore, the reaction time for transannulation of N-heteroaryl aldehydes or ketones was optimized as 10 h.

Effect of Temperature. Temperature is one of the significant parameters which play a vital role in influencing the thermodynamic activities of the reaction. In order to determine the most favorable reaction conditions using Cu@AA@APTES@GO as a catalyst, the test reaction was carried out at diverse range of temperatures (40−80 °C). The

DOI: 10.1021/acsomega.8b02902
ACS Omega 2019, 4, 3146−3158

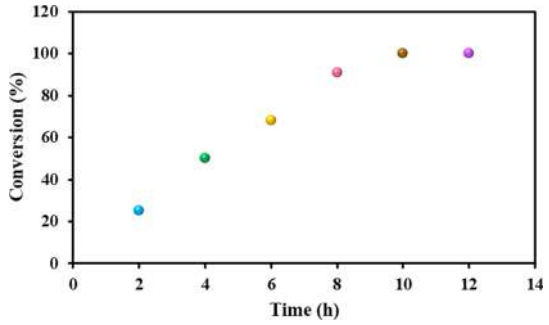

Figure 9. Effect of time on the transannulation of N-heteroaryl aldehydes or ketones [reaction conditions: 2-acetylpyridine (0.10 mmol), benzyl amine (0.10 mmol), acetonitrile (2 mL), catalyst (15 mg), 80 °C].

conversion percentage has been represented as a function of temperature (Supporting Information Figure S6). Compared with the results obtained at 80 °C, a lower conversion of 35% to the desired product was obtained at 60 °C, suggesting that the catalytic activity of the graphene oxide-based copper nanocatalyst decreased by decreasing the reaction temperature. As expected, no desired product was formed at room temperature. Notably, the optimized temperature for the synthesis of imidazo[1,5-*a*]pyridines was 80 °C.

Effect of Solvents. Nature of solvents has a remarkable impact on conversion percentage of the desired products. Therefore, in order to study their effect on the concerned reaction, test substrates were subjected to different polar and nonpolar solvents. First, the test reaction was carried out in polar solvents (ethanol and acetonitrile) which resulted in 73 and 100% of desired product, whereas in the presence of nonpolar solvents (hexane and toluene), only 57 and 63% of conversion percentage were obtained (Figure 10). In fact,

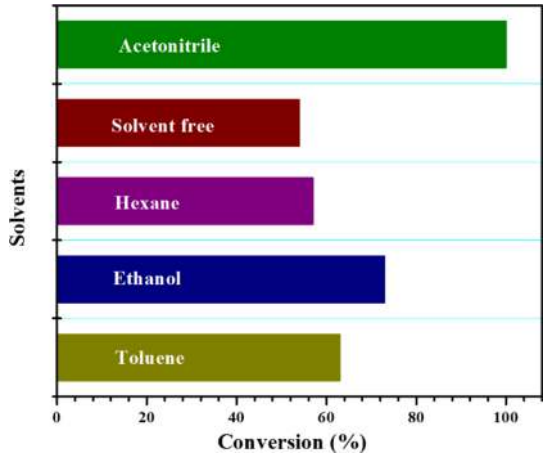

Figure 10. Effect of solvents on the transannulation of N-heteroaryl aldehydes or ketones [reaction conditions: 2-acetylpyridine (0.10 mmol), benzyl amine (0.10 mmol), solvent (2 mL), catalyst (15 mg), 10 h, 80 °C].

lowest conversion percentage was observed when the experiment was run in solvent-free conditions, even if the reaction was carried out for a prolonged period of time. Therefore, the order of reactivity in different solvents was found to be acetonitrile > ethanol > toluene > hexane > solvent-free.

Scope of Substrates. On the basis of these promising screening results, we next scrutinized the scope of the current procedure by testing several pyridine aldehyde or ketone derivatives and amines using the graphene oxide-supported copper catalyst. First, we evaluated the scope of amine derivatives bearing either electron-donating or electron-withdrawing groups under the optimized reaction conditions, and the results are demonstrated in Table 1. It was found that amines containing electron-withdrawing or electron-donating groups gave moderate to good conversion percentages of the desired products. Subsequently, a series of N-heterocyclic aldehydes or ketones were examined as reaction partners. The results indicated that a diverse range of N-heterocyclic aldehydes or ketones were all compatible with this transformation showing moderate to good conversion percentages. The most important feature of the present approach is that this tandem reaction is devoid of unwanted side products.

Mechanism. A plausible catalytic cycle on the basis of previous literature reports has been proposed and is shown in Scheme 2. First, the condensation reaction between N-heteroarene aldehyde or ketone and alkylamine generates complex A.[32] In the next step, complex B is formed via the coordinative interaction of copper(II) with the pyridyl N-atom of complex A. Thereafter, oxidative dehydrogenation of complex B in the presence of copper(II) generates complex C which undergoes isomerization to give complex D that eventually eliminates the imidazo[1,5-*a*]pyridine product by giving Cu species. Finally, the catalyst is regenerated back via the removal of water.[77]

Catalytic Activity Tests. Reusability of a catalyst is an important aspect from the commercial point of view as it increases the potentiality of the catalyst. In order to take advantage of the heterogeneous nature, the recyclability of the Cu@AA@APTES@GO nanocatalyst was investigated for the test reaction. In order to do so, after completion of the reaction, the catalyst was easily recovered from the reaction media by means of centrifugation and used for the next catalytic cycles without any additional treatment. Thanks to the high stability of the graphene oxide-supported copper nanocatalyst that could catalyze the full conversion of test substrates during all repeated cycles without any significant loss in catalytic activity (Figure 11). This observation was further supported by SEM, TEM, and FT-IR analysis of the recovered catalyst (Figures S1, S2, and S7) which showed that the structure of recovered catalyst remained unchanged in comparison to fresh catalyst that provided a concrete proof of the excellent stability of the catalyst.

In order to verify that the observed catalysis was due to the graphene oxide-supported copper nanocatalyst rather than leached copper species in solution, a hot filtration experiment of test reaction was carried out. The solid catalyst was removed from the reaction mixture with the assistance of centrifugation after 5 h (half the reaction time), and the reaction was continued with the solid-free filtrate for an additional 5 h. Subsequently, the supernatant was analyzed by GC−MS in order to find out the conversion percentage, and it was observed that the reaction had reached 62% completion at the end of 5 h. There was no appreciable change in the conversion percentage of the desired product when the supernatant was subjected to further stirring after removing the solid catalyst from it. The GC−MS results showed that the reaction was hard to occur even after prolonged time as the removal of catalyst had stopped the reactivity. Thus, these results demonstrated that there was no loss of catalytic components during the course of reaction.

DOI: 10.1021/acsomega.8b02902
ACS Omega 2019, 4, 3146−3158

Table 1. Transannulation of N-Heterocyclic Aldehydes or Ketones and Alkylamines Using Cu@AA@APTES@GO as a Catalyst[a]

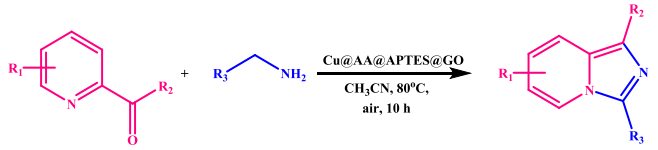

Entry	N-heteroaryl aldehydes or ketones	Alkylamines	Product	[b]Conversion %	[c]TON
1.	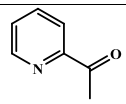	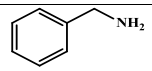	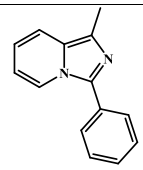	100	529
2.	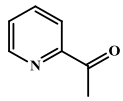	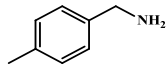	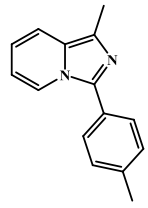	76	402
3.	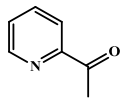	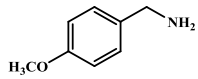	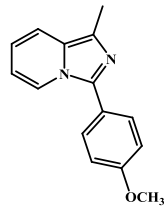	100	529
4.	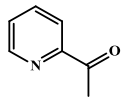	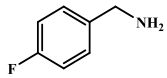	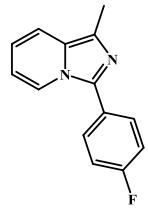	80	423
5.	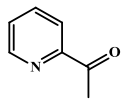	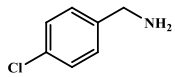	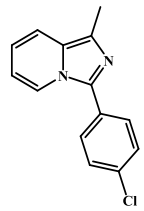	40	212
6.	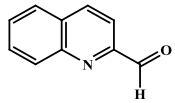	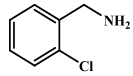	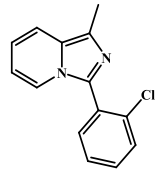	68	360
7.	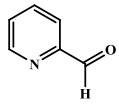	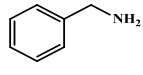	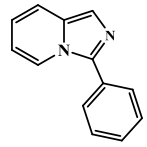	98	518

DOI: 10.1021/acsomega.8b02902
ACS Omega 2019, 4, 3146−3158

Table 1. continued

Entry	N-heteroaryl aldehydes or ketones	Alkylamines	Product	[b]Conversion %	[c]TON
8.	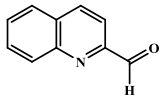	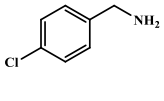	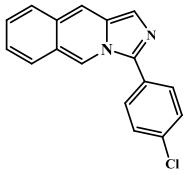	35	185
9.	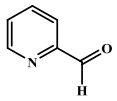	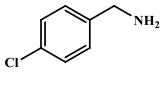	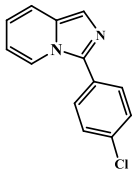	40	212
10.	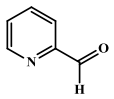	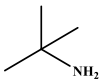	-	-	-
11.	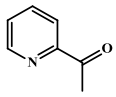	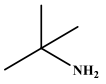	-	-	-

[a]Reaction conditions: N-heteroaryl aldehydes or ketones (0.10 mmol), alkylamines (0.10 mmol), acetonitrile (2 mL), catalyst (15 mg), 10 h, 80 °C. [b]Conversion percentage was determined by GC−MS. [c]TON is the number of moles of product per mole of catalyst.

Scheme 2. Plausible Mechanism for the Transannulation of N-Heterocyclic Aldehydes and Alkylamines Using Cu@AA@APTES@GO as a Catalyst

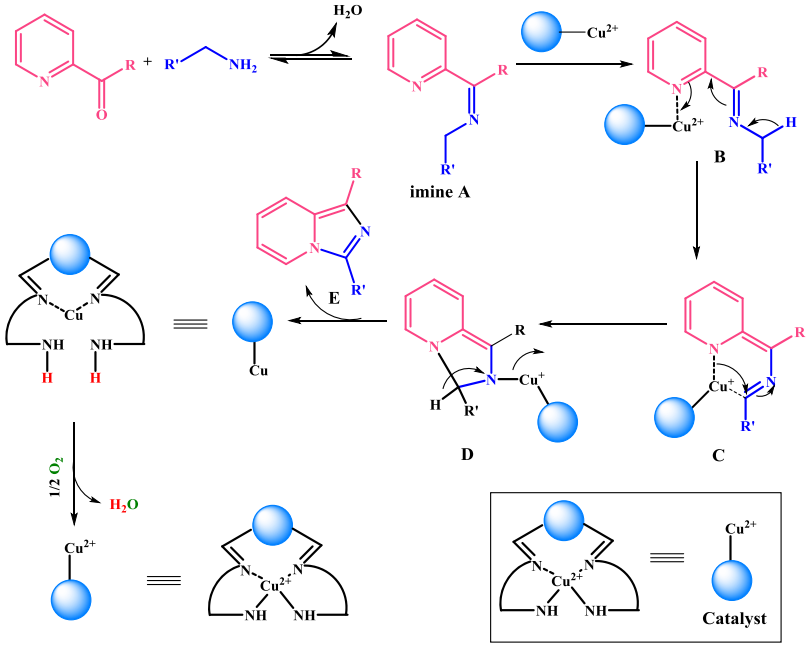

Comparison of the Catalytic Activity of Cu@AA@APTES@GO with the Previously Reported Catalytic Systems. In order to compare the advantages of the present approach, an extensive study of previous literature precedents was carried out for the transannulation of N-heteroaryl aldehydes or ketones with alkylamines. It is important to note that all of the earlier catalysts employed for the concerned reaction were homogeneous and had serious limitations. A homogeneous catalyzed reaction mixture could lead to the formation of inactive dimers or aggregates which obstructed the catalytic active sites, thereby hampering its activity. Besides, it is clearly evident from Table 2 that graphene oxide-based copper catalyst revealed good catalytic results in comparison to other catalysts employed till date. Moreover, homogeneous catalysts could not be recovered as they undergo decomposition immediately after the completion of the reaction and could not be reused for further cycles. On the contrary, the graphene oxide-based copper nanocatalysts could be recovered easily via centrifugation and recycled for six

DOI: 10.1021/acsomega.8b02902
ACS Omega 2019, 4, 3146−3158

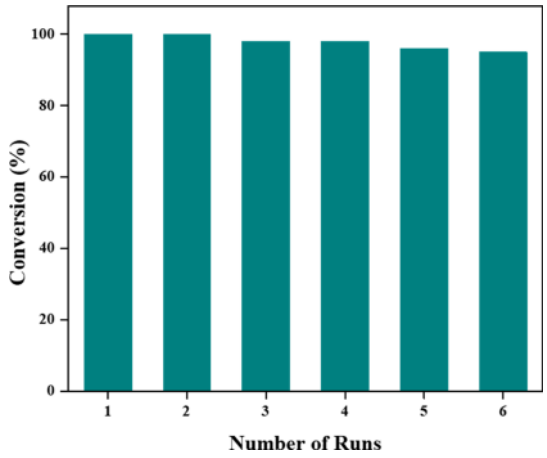

Figure 11. Catalyst recycle runs for the transannulation of N-heterocyclic aldehydes and alkylamines [reaction conditions: 2-acetylpyridine (0.10 mmol), benzyl amine (0.10 mmol), acetonitrile (2 mL), catalyst (15 mg), 10 h, 80 °C].

consecutive cycles without any significant loss in its catalytic activity.

CONCLUSIONS

In summary, we have successfully developed a new heterogeneous catalyst that is composed of exfoliated 2D graphene oxide-based nanomaterial for transannulation of N-heteroaryl aldehydes or ketones with alkylamines. We employed a simple and general route for the immobilization of copper complex onto amine-functionalized graphene oxide nanosheets for the synthesis of the Cu@AA@APTES@GO nanocatalyst. The presence of abundant oxygenated hydroxyl functional groups on basal planes of exfoliated 2D graphene oxide nanocomposites provides very effective and powerful sites for the loading of Schiff base metal complex. It exhibits significantly improved catalytic efficiencies which could be accredited to the presence of nanometer size of support material and 2D confinement that provides a large number of catalytically active sites. Further, the efficacy of the synthesized Cu@AA@APTES@GO catalyst can also be realized by focusing on the results of various catalytic activity tests conducted which include simple work up procedure, substrate scope, hot filtration, and recyclability experiments. Consequently, this methodology offers a new approach for the transannulation of N-heteroaryl aldehydes or ketones with alkylamines using graphene oxide-supported copper catalyst under mild reaction conditions.

ASSOCIATED CONTENT

Supporting Information

The Supporting Information is available free of charge on the ACS Publications website at DOI: 10.1021/acsomega.8b02902.

SEM and TEM images of the recovered Cu@AA@APTES@GO catalyst; C 1s and N 1s XPS spectra of the catalyst; elemental mapping and ED-XRF of Cu@AA@APTES@GO; screening of various catalysts and effect of temperature on the transannulation of N-heteroaryl aldehydes or ketones with alkylamines; FT-IR spectrum of recovered catalyst; GC−MS chromatogram of the test substrates; and mass spectra of synthesized products (PDF)

AUTHOR INFORMATION

Corresponding Author

*E-mail: rksharmagreenchem@hotmail.com. Phone: 011-276666250. Fax: +91-011-27666250.

ORCID

Rakesh K. Sharma: 0000-0003-4281-876X

Table 2. Comparison of Catalytic Activity of Cu@AA@APTES@GO with Other Catalyst Reported in the Literature for Transannulation of N-Heteroaryl Aldehydes or Ketones with Alkylamines

Entry	N-heteroaryl aldehydes or ketones	Alkylamines	Reaction parameters	Yield/ Conversion %	References
1.	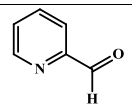	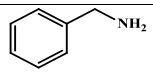	CuBr (20 mol %), air, CH_3CN, 80 °C, 24 h	85	[30]
2.	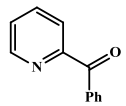	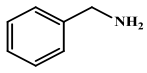	$Cu(OAc)_2.H_2O$, air, DMF, 110 °C, 24 h	77	[31]
3.	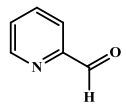	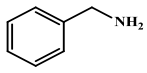	Cu@AA@APTES@GO, air, CH_3CN, 80 °C, 10 h	98	Present work
4.	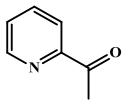	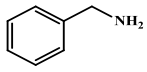	Cu@AA@APTES@GO, air, CH_3CN, 80 °C, 10 h	100	Present work

DOI: 10.1021/acsomega.8b02902
ACS Omega 2019, 4, 3146−3158

Notes

The authors declare no competing financial interest.

■ ACKNOWLEDGMENTS

One of the authors A.S. thanks the Council of Scientific and Industrial Research (CSIR), New Delhi, India, for the award of Senior Research fellowship. The author also thanks USIC-CIL, DU for FT-IR, SEM, TEM, and XRD and Catalysis Center for Energy Innovation, University of Delaware, USA, for providing instrumentation facilities for XPS analysis.

■ REFERENCES

(1) He, G.; Zhao, Y.; Zhang, S.; Lu, C.; Chen, G. Highly efficient syntheses of azetidines, pyrrolidines, and indolines via palladium catalyzed intramolecular amination of C (sp^3)−H and C (sp^2)−H bonds at γ and δ positions. *J. Am. Chem. Soc.* **2011**, *134*, 3−6.

(2) Wasa, M.; Chan, K. S. L.; Zhang, X.-G.; He, J.; Miura, M.; Yu, J.-Q. Ligand-enabled methylene C (sp^3)−H bond activation with a Pd (II) catalyst. *J. Am. Chem. Soc.* **2012**, *134*, 18570−18572.

(3) Zhu, R.-Y.; He, J.; Wang, X.-C.; Yu, J.-Q. Ligand-promoted alkylation of C (sp^3)−H and C (sp^2)−H bonds. *J. Am. Chem. Soc.* **2014**, *136*, 13194−13197.

(4) Lin, Y.; Xu, H.; Gong, L.; Wen, T. B.; He, X.-M.; Xia, H. C−H Bond Activation and Subsequent C(sp^2)−C(sp^3) Bond Formation: Coupling of Bromomethyl and Triphenylphosphine in an Iridium Complex. *Organometallics* **2010**, *29*, 2904−2910.

(5) Shang, R.; Ilies, L.; Asako, S.; Nakamura, E. Iron-Catalyzed C (sp^2)−H Bond Functionalization with Organoboron Compounds. *J. Am. Chem. Soc.* **2014**, *136*, 14349−14352.

(6) Gao, P.; Guo, W.; Xue, J.; Zhao, Y.; Yuan, Y.; Xia, Y.; Shi, Z. Iridium(III)-Catalyzed Direct Arylation of C-H Bonds with Diaryliodonium Salts. *J. Am. Chem. Soc.* **2015**, *137*, 12231−12240.

(7) Roane, J.; Daugulis, O. A General Method for Aminoquinoline-Directed, Copper-Catalyzed sp^2 C−H Bond Amination. *J. Am. Chem. Soc.* **2016**, *138*, 4601−4607.

(8) Zhou, B.; Hu, Y.; Wang, C. Manganese-Catalyzed Direct Nucleophilic C (sp^2)−H Addition to Aldehydes and Nitriles. *Angew. Chem.* **2015**, *127*, 13863−13867.

(9) Liu, C.; Zhang, Q.; Li, H.; Guo, S.; Xiao, B.; Deng, W.; Liu, L.; He, W. Cu/Fe Catalyzed Intermolecular Oxidative Amination of Benzylic C−H Bonds. *Chem.—Eur. J.* **2016**, *22*, 6208−6212.

(10) He, G.; Chatani, N. Catalytic Functionalization of C (sp^2)- H and C (sp^3)- H Bonds by Using Bidentate Directing Groups. *Angew. Chem., Int. Ed.* **2013**, *52*, 11726−11743.

(11) Wu, X.; Zhao, Y.; Ge, H. Direct Aerobic Carbonylation of C (sp^2)−H and C (sp^3)−H Bonds through Ni/Cu Synergistic Catalysis with DMF as the Carbonyl Source. *J. Am. Chem. Soc.* **2015**, *137*, 4924−4927.

(12) Ramirez, T. A.; Zhao, B.; Shi, Y. Recent advances in transition metal-catalyzed sp ^{3} C−H amination adjacent to double bonds and carbonyl groups. *Chem. Soc. Rev.* **2012**, *41*, 931−942.

(13) Collet, F.; Lescot, C.; Dauban, P. Catalytic C-H amination: the stereoselectivity issue. *Chem. Soc. Rev.* **2011**, *40*, 1926−1936.

(14) Pan, J.; Su, M.; Buchwald, S. L. Palladium(0)-Catalyzed Intermolecular Amination of Unactivated C sp 3H Bonds. *Angew. Chem.* **2011**, *123*, 8806−8810.

(15) Bess, E. N.; DeLuca, R. J.; Tindall, D. J.; Oderinde, M. S.; Roizen, J. L.; Du Bois, J.; Sigman, M. S. Analyzing site selectivity in $Rh_2(esp)_2$ catalyzed intermolecular C−H amination reactions. *J. Am. Chem. Soc.* **2014**, *136*, 5783−5789.

(16) Liang, C.; Robert-Peillard, F.; Fruit, C.; Müller, P.; Dodd, R. H.; Dauban, P. Efficient Diastereoselective Intermolecular Rhodium-Catalyzed C−H Amination. *Angew. Chem., Int. Ed.* **2006**, *45*, 4641−4644.

(17) Zhang, J.; Zhu, D.; Yu, C.; Wan, C.; Wang, Z. A Simple and Efficient Approach to the Synthesis of 2-Phenylquinazolines via sp^3 C− H Functionalization. *Org. Lett.* **2010**, *12*, 2841−2843.

(18) Yan, Y.; Zhang, Y.; Zha, Z.; Wang, Z. Mild Metal-Free Sequential Dual Oxidative Amination of C (sp^3)−H bonds: Efficient Synthesis of Imidazo [1, 5-a] pyridines. *Org. Lett.* **2013**, *15*, 2274−2277.

(19) Kamal, A.; Rao, A. V. S.; Nayak, V. L.; Reddy, N. V. S.; Swapna, K.; Ramakrishna, G.; Alvala, M. Synthesis and biological evaluation of imidazo[1,5-a]pyridine-benzimidazole hybrids as inhibitors of both tubulin polymerization and PI3K/Akt pathway. *Org. Biomol. Chem.* **2014**, *12*, 9864−9880.

(20) Khan, M. S.; Baig, M. H.; Ahmad, S.; Siddiqui, S. A.; Srivastava, A. K.; Srinivasan, K. V.; Ansari, I. A. Design, Synthesis, Evaluation and Thermodynamics of 1-Substituted Pyridylimidazo[1,5-a]Pyridine Derivatives as Cysteine Protease Inhibitors. *PLoS One* **2013**, *8*, No. e69982.

(21) Pelletier, G.; Charette, A. B. Triflic Anhydride Mediated Synthesis of Imidazo[1,5-a]azines. *Org. Lett.* **2013**, *15*, 2290−2293.

(22) Shibahara, F.; Kitagawa, A.; Yamaguchi, E.; Murai, T. Synthesis of 2-Azaindolizines by Using an Iodine-Mediated Oxidative Desulfurization Promoted Cyclization ofN-2-Pyridylmethyl Thioamides and an Investigation of Their Photophysical Properties. *Org. Lett.* **2006**, *8*, 5621−5624.

(23) Wang, Q.; Zhang, S.; Guo, F.; Zhang, B.; Hu, P.; Wang, Z. Natural α-Amino Acids Applied in the Synthesis of Imidazo[1,5-a]N-heterocycles under Mild Conditions. *J. Org. Chem.* **2012**, *77*, 11161−11166.

(24) Shi, Y.; Gulevich, A. V.; Gevorgyan, V. Rhodium-Catalyzed NH Insertion of Pyridyl Carbenes Derived from Pyridotriazoles: A General and Efficient Approach to 2-Picolylamines and Imidazo-[1,5-a]pyridines. *Angew. Chem., Int. Ed.* **2014**, *53*, 14191−14195.

(25) Li, Y.; Chao, A.; Fleming, F. F. Isonitrile alkylations: a rapid route to imidazo[1,5-a]pyridines. *Chem. Commun.* **2016**, *52*, 2111−2113.

(26) Murai, T.; Nagaya, E.; Shibahara, F.; Maruyama, T. Imidazo[1,5-a]pyridine-1-ylalkylalcohols: synthesis via intramolecular cyclization of N-thioacyl 1,2-aminoalcohols and their silyl ethers and molecular structures. *Org. Biomol. Chem.* **2012**, *10*, 4943−4953.

(27) Shibahara, F.; Sugiura, R.; Yamaguchi, E.; Kitagawa, A.; Murai, T. Synthesis of Fluorescent 1,3-Diarylated Imidazo[1,5-a]pyridines: Oxidative Condensation−Cyclization of Aryl-2-Pyridylmethylamines and Aldehydes with Elemental Sulfur as an Oxidant. *J. Org. Chem.* **2009**, *74*, 3566−3568.

(28) Yamaguchi, E.; Shibahara, F.; Murai, T. 1-Alkynyl- and 1-Alkenyl-3-arylimidazo[1,5-a]pyridines: Synthesis, Photophysical Properties, and Observation of a Linear Correlation between the Fluorescent Wavelength and Hammett Substituent Constants. *J. Org. Chem.* **2011**, *76*, 6146−6158.

(29) Alcarazo, M.; Roseblade, S. J.; Cowley, A. R.; Fernández, R.; Brown, J. M.; Lassaletta, J. M. Imidazo[1,5-a]pyridine: A Versatile Architecture for Stable N-Heterocyclic Carbenes. *J. Am. Chem. Soc.* **2005**, *127*, 3290−3291.

(30) Crawforth, J. M.; Paoletti, M. A one-pot synthesis of imidazo[1,5-a]pyridines. *Tetrahedron Lett.* **2009**, *50*, 4916−4918.

(31) Li, M.; Xie, Y.; Ye, Y.; Zou, Y.; Jiang, H.; Zeng, W. Cu (I)-Catalyzed Transannulation of N-Heteroaryl Aldehydes or Ketones with Alkylamines via C (sp^3)−H Amination. *Org. Lett.* **2014**, *16*, 6232−6235.

(32) Wang, H.; Xu, W.; Wang, Z.; Yu, L.; Xu, K. Copper-Catalyzed Oxidative Amination of sp^3 C−H Bonds under Air: Synthesis of 1, 3-Diarylated Imidazo [1, 5-a] pyridines. *J. Org. Chem.* **2015**, *80*, 2431−2435.

(33) Joshi, A.; Chandra Mohan, D.; Adimurthy, S. Copper-Catalyzed Denitrogenative Transannulation Reaction of Pyridotriazoles: Synthesis of Imidazo[1,5-a]pyridines with Amines and Amino Acids. *Org. Lett.* **2016**, *18*, 464−467.

(34) Wang, H.; Xu, W.; Xin, L.; Liu, W.; Wang, Z.; Xu, K. Synthesis of 1,3-Disubstituted Imidazo[1,5-a]pyridines from Amino Acids via Catalytic Decarboxylative Intramolecular Cyclization. *J. Org. Chem.* **2016**, *81*, 3681−3687.

DOI: 10.1021/acsomega.8b02902
ACS Omega 2019, 4, 3146−3158

(35) Bluhm, M. E.; Ciesielski, M.; Görls, H.; Döring, M. Copper-Catalyzed Oxidative Heterocyclization by Atmospheric Oxygen. *Angew. Chem., Int. Ed.* **2002**, *41*, 2962−2965.
(36) Li, L.; Zhu, Y.; Lu, X.; Wei, M.; Zhuang, W.; Yang, Z.; Feng, X. Carbon heterogeneous surface modification on a mesoporous TiO_2-supported catalyst and its enhanced hydrodesulfurization performance. *Chem. Commun.* **2012**, *48*, 11525−11527.
(37) Dang, T. T.; Zhu, Y.; Ngiam, J. S. Y.; Ghosh, S. C.; Chen, A.; Seayad, A. M. Palladium nanoparticles supported on ZIF-8 as an efficient heterogeneous catalyst for aminocarbonylation. *ACS Catal.* **2013**, *3*, 1406−1410.
(38) Julkapli, N. M.; Bagheri, S. Graphene supported heterogeneous catalysts: an overview. *Int. J. Hydrog. Energy* **2015**, *40*, 948−979.
(39) Gawande, M. B.; Branco, P. S.; Varma, R. S. Nano-magnetite (Fe_3O_4) as a support for recyclable catalysts in the development of sustainable methodologies. *Chem. Soc. Rev.* **2013**, *42*, 3371−3393.
(40) Gan, W.; Dyson, P. J.; Laurenczy, G. Heterogeneous Silica-Supported Ruthenium Phosphine Catalysts for Selective Formic Acid Decomposition. *ChemCatChem* **2013**, *5*, 3124−3130.
(41) Aghapoor, K.; Ebadi-Nia, L.; Mohsenzadeh, F.; Mohebi Morad, M.; Balavar, Y.; Darabi, H. R. Silica-supported bismuth(III) chloride as a new recyclable heterogeneous catalyst for the Paal-Knorr pyrrole synthesis. *J. Org. Chem.* **2012**, *708*−*709*, 25−30.
(42) Kawamorita, S.; Murakami, R.; Iwai, T.; Sawamura, M. Synthesis of primary and secondary alkylboronates through site-selective C (sp^3)−H activation with silica-supported monophosphine−Ir catalysts. *J. Am. Chem. Soc.* **2013**, *135*, 2947−2950.
(43) Basu, B.; Paul, S. An improved preparation of mesoporous silica-supported Pd as sustainable catalysts for phosphine-free Suzuki−Miyaura and Heck coupling reactions. *Appl. Organomet. Chem.* **2013**, *27*, 588−594.
(44) Dave, S. H.; Gong, C.; Robertson, A. W.; Warner, J. H.; Grossman, J. C. Chemistry and structure of graphene oxide via direct imaging. *ACS Nano* **2016**, *10*, 7515−7522.
(45) Zaharie-Butucel, D.; Potara, M.; Craciun, A. M.; Boukherroub, R.; Szunerits, S.; Astilean, S. Revealing the structure and functionality of graphene oxide and reduced graphene oxide/pyrene carboxylic acid interfaces by correlative spectral and imaging analysis. *Phys. Chem. Chem. Phys.* **2017**, *19*, 16038−16046.
(46) Nekahi, A.; Marashi, S. P. H.; Fatmesari, D. H. Modified structure of graphene oxide by investigation of structure evolution. *Bull. Mater. Sci.* **2015**, *38*, 1717−1722.
(47) Quintana, M.; Vazquez, E.; Prato, M. Organic functionalization of graphene in dispersions. *Acc. Chem. Res.* **2012**, *46*, 138−148.
(48) Deng, D.; Novoselov, K. S.; Fu, Q.; Zheng, N.; Tian, Z.; Bao, X. Catalysis with two-dimensional materials and their heterostructures. *Nat. Nanotechnol.* **2016**, *11*, 218.
(49) Dutta, S.; Sharma, S.; Sharma, A.; Sharma, R. K. Fabrication of Core-Shell-Structured Organic-Inorganic Hybrid Nanocatalyst for the Expedient Synthesis of Polysubstituted Oxazoles via Tandem Oxidative Cyclization Pathway. *ACS Omega* **2017**, *2*, 2778−2791.
(50) Gupta, R.; Yadav, M.; Gaur, R.; Arora, G.; Sharma, R. K. A straightforward one-pot synthesis of bioactive N-aryl oxazolidin-2-ones via a highly efficient Fe_3O_4@SiO_2-supported acetate-based butylimidazolium ionic liquid nanocatalyst under metal-and solvent-free conditions. *Green Chem.* **2017**, *19*, 3801−3812.
(51) Sharma, R. K.; Yadav, M.; Monga, Y.; Gaur, R.; Adholeya, A.; Zboril, R.; Varma, R. S.; Gawande, M. B. Silica-Based Magnetic Manganese Nanocatalyst - Applications in the Oxidation of Organic Halides and Alcohols. *ACS Sustain. Chem. Eng.* **2016**, *4*, 1123−1130.
(52) Sharma, R. K.; Dhingra, S. Designing and Synthesis of Functionalized Silica Gels and their Applications as Metal Scavengers. *Sensors, and Catalysts: Green Chemistry Approach*; LAP Lambert Academic Publishing: Germany, 2011.
(53) Sharma, R. K.; Dutta, S.; Sharma, S.; Zboril, R.; Varma, R. S.; Gawande, M. B. Fe_3O_4 (iron oxide)-supported nanocatalysts: synthesis, characterization and applications in coupling reactions. *Green Chem.* **2016**, *18*, 3184−3209.
(54) Sharma, R. K.; Sharma, A.; Sharma, S.; Dutta, S. Unprecedented Ester-Amide Exchange Reaction Using Highly Versatile Two-Dimensional Graphene Oxide Supported Base Metal Nanocatalyst. *Ind. Eng. Chem. Res.* **2018**, *57*, 3617−3627.
(55) Hummers, W. S., Jr.; Offeman, R. E. Preparation of graphitic oxide. *J. Am. Chem. Soc.* **1958**, *80*, 1339.
(56) Bai, C.; Zhao, Q.; Li, Y.; Zhang, G.; Zhang, F.; Fan, X. Palladium complex immobilized on graphene oxide as an efficient and recyclable catalyst for Suzuki coupling reaction. *Catal. Lett.* **2014**, *144*, 1617−1623.
(57) El-Ghamaz, N. A.; Ghoneim, M. M.; El-Sonbati, A. Z.; Diab, M. A.; El-Bindary, A. A.; Abd El-Kader, M. K. Synthesis and optical properties studies of antipyrine derivatives thin films. *J. Saudi Chem. Soc.* **2017**, *21*, S339−S348.
(58) Chandra, S.; Jain, D.; Sharma, A. K.; Sharma, P. Coordination Modes of a Schiff Base Pentadentate Derivative of 4-Aminoantipyrine with Cobalt(II), Nickel(II) and Copper(II) Metal Ions: Synthesis, Spectroscopic and Antimicrobial Studies. *Molecules* **2009**, *14*, 174−190.
(59) Paul, S.; Clark, J. H. Structure-activity relationship between some novel silica supported palladium catalysts: a study of the Suzuki reaction. *J. Mol. Catal. A: Chem.* **2004**, *215*, 107−111.
(60) Gnana kumar, G.; Kirubaharan, C. J.; Udhayakumar, S.; Ramachandran, K.; Karthikeyan, C.; Renganathan, R.; Nahm, K. S. Synthesis, structural, and morphological characterizations of reduced graphene oxide-supported polypyrrole anode catalysts for improved microbial fuel cell performances. *ACS Sustain. Chem. Eng.* **2014**, *2*, 2283−2290.
(61) Su, H.; Wu, S.; Li, Z.; Huo, Q.; Guan, J.; Kan, Q. Co(II), Fe(III) or VO(II) Schiff base metal complexes immobilized on graphene oxide for styrene epoxidation. *Appl. Organomet. Chem.* **2015**, *29*, 462−467.
(62) Lin, S.; Dong, L.; Zhang, J.; Lu, H. Room-Temperature Intercalation and ∼1000-Fold Chemical Expansion for Scalable Preparation of High-Quality Graphene. *Chem. Mater.* **2016**, *28*, 2138−2146.
(63) Kumar, A.; Rout, L.; Achary, L. S. K.; Dhaka, R. S.; Dash, P. Greener Route for Synthesis of aryl and alkyl-14H-dibenzo [aj] xanthenes using Graphene Oxide-Copper Ferrite Nanocomposite as a Recyclable Heterogeneous Catalyst. *Sci. Rep.* **2017**, *7*, 42975.
(64) Mungse, H. P.; Verma, S.; Kumar, N.; Sain, B.; Khatri, O. P. Grafting of oxo-vanadium Schiff base on graphene nanosheets and its catalytic activity for the oxidation of alcohols. *J. Mater. Chem.* **2012**, *22*, 5427−5433.
(65) Sitko, R.; Janik, P.; Feist, B.; Talik, E.; Gagor, A. Suspended aminosilanized graphene oxide nanosheets for selective preconcentration of lead ions and ultrasensitive determination by electrothermal atomic absorption spectrometry. *ACS Appl. Mater. Interfaces* **2014**, *6*, 20144−20153.
(66) Gemeay, A. H.; El-Halwagy, M. E.; El-Sharkawy, R. G.; Zaki, A. B. Chelation mode impact of copper(II)-aminosilane complexes immobilized onto graphene oxide as an oxidative catalyst. *J. Environ. Chem. Eng.* **2017**, *5*, 2761−2772.
(67) Dai, K.; Sun, S.; Xu, W.; Song, Y.; Deng, Z.; Qian, X. Covalently-functionalized graphene oxide via introduction of bifunctional phosphorus-containing molecules as an effective flame retardant for polystyrene. *RSC Adv.* **2018**, *8*, 24993−25000.
(68) Zhu, Y.; Shi, Y.; Huang, Z.; Duan, L.; Hu, Y.; Gong, X. Preparation of Schiff base decorated graphene oxide and its application in TPU with enhanced thermal stability. *RSC Adv.* **2016**, *6*, 90018−90023.
(69) Kumari, S.; Shekhar, A.; Pathak, D. D. Synthesis and characterization of a Cu(ii) Schiff base complex immobilized on graphene oxide and its catalytic application in the green synthesis of propargylamines. *RSC Adv.* **2016**, *6*, 15340−15344.
(70) Pourjavadi, A.; Safaie, N.; Hosseini, S. H.; Bennett, C. Graphene oxide/poly(vinyl imidazole) nanocomposite: an effective support for preparation of highly loaded heterogeneous copper catalyst. *Appl. Organomet. Chem.* **2015**, *29*, 601−607.

DOI: 10.1021/acsomega.8b02902
ACS Omega 2019, 4, 3146−3158

(71) Li, Z.; Wu, S.; Ding, H.; Zheng, D.; Hu, J.; Wang, X.; Huo, Q.; Guan, J.; Kan, Q. Immobilized Cu(ii) and Co(ii) salen complexes on graphene oxide and their catalytic activity for aerobic epoxidation of styrene. *New J. Chem.* **2013**, *37*, 1561−1568.
(72) Zhao, Q.; Bai, C.; Zhang, W.; Li, Y.; Zhang, G.; Zhang, F.; Fan, X. Catalytic epoxidation of olefins with graphene oxide supported copper (Salen) complex. *Ind. Eng. Chem. Res.* **2014**, *53*, 4232−4238.
(73) Khatri, P. K.; Choudhary, S.; Singh, R.; Jain, S. L.; Khatri, O. P. Grafting of a rhenium-oxo complex on Schiff base functionalized graphene oxide: an efficient catalyst for the oxidation of amines. *Dalton Trans.* **2014**, *43*, 8054−8061.
(74) Díez-Betriu, X.; Álvarez-García, S.; Botas, C.; Álvarez, P.; Sánchez-Marcos, J.; Prieto, C.; Menéndez, R.; de Andrés, A. Raman spectroscopy for the study of reduction mechanisms and optimization of conductivity in graphene oxide thin films. *J. Mater. Chem. C* **2013**, *1*, 6905−6912.
(75) López-Díaz, D.; López Holgado, M.; García-Fierro, J. L.; Velázquez, M. M. Evolution of the Raman Spectrum with the Chemical Composition of Graphene Oxide. *J. Phys. Chem. C* **2017**, *121*, 20489−20497.
(76) Hsiao, M.-C.; Liao, S.-H.; Yen, M.-Y.; Liu, P.-I.; Pu, N.-W.; Wang, C.-A.; Ma, C.-C. M. Preparation of covalently functionalized graphene using residual oxygen-containing functional groups. *ACS Appl. Mater. Interfaces* **2010**, *2*, 3092−3099.
(77) Bluhm, M. E.; Ciesielski, M.; Görls, H.; Döring, M. Copper-Catalyzed Oxidative Heterocyclization by Atmospheric Oxygen. *Angew. Chem., Int. Ed.* **2002**, *41*, 2962−2965.

DOI: 10.1021/acsomega.8b02902
ACS Omega 2019, 4, 3146−3158